

Article

Safety Assessment and Crash Compatibility of Heavy Quadricycle under Frontal Impact Collisions

Suphanut Kongwat ¹, Thonn Homsnit ¹ , Chaimongkol Padungtree ¹, Naphon Tonitwong ¹, Pornkasem Jongpradist ²  and Pattaramon Jongpradist ^{1,3,*} 

¹ Department of Mechanical Engineering, Faculty of Engineering, King Mongkut's University of Technology Thonburi, Bangkok 10140, Thailand

² Construction Innovations and Future Infrastructures Research Center, Department of Civil Engineering, Faculty of Engineering, King Mongkut's University of Technology Thonburi, Bangkok 10140, Thailand

³ Mobility and Vehicle Technology Research Center, King Mongkut's University of Technology Thonburi, Bangkok 10140, Thailand

* Correspondence: pattaramon.tan@kmutt.ac.th; Tel.: +66-24-709-275

Abstract: An electric heavy quadricycle, categorized as an L7e vehicle, is an alternative solution for sustainable mobility with a lower carbon footprint and high energy consumption efficiency. However, accidental crashes of quadricycles with larger vehicle opponents can cause extensive damage to their structures and fatal injury to the occupants due to their geometry drawback in limited space in the front crumple zone. This work investigates the crashworthiness performance and safety assessment of the L7e vehicle under rigid wall crash tests and crash compatibility in car-to-car collisions with a sedan and an SUV. Crash scenarios are simulated using a nonlinear finite element analysis via LS-DYNA to evaluate structural crashworthiness and occupant injuries of a hybrid III 50th percentile male dummy. The compatible vertical alignment of the primary energy-absorbing structure substantially affects the safety of the quadricycle under a frontal crash. A secondary energy-absorbing component should be adapted to the L7e vehicle to achieve vertical alignment with different vehicle sizes. In addition, the typical rigid-wall frontal crash test at 50 kph considerably underestimates the structural damage and occupant injury of the L7e vehicle compared to car-to-car collisions. Thus, additional crash tests representing car-to-car collisions that account for the car's smaller size and lighter mass should be included in the safety regulation for the L7e vehicle.

Keywords: frontal crash; heavy quadricycle; structural crashworthiness; crash compatibility; occupant safety



Citation: Kongwat, S.; Homsnit, T.; Padungtree, C.; Tonitwong, N.; Jongpradist, P.; Jongpradist, P. Safety Assessment and Crash Compatibility of Heavy Quadricycle under Frontal Impact Collisions. *Sustainability* **2022**, *14*, 13458. <https://doi.org/10.3390/su142013458>

Academic Editor: Ocktaeck Lim

Received: 24 August 2022

Accepted: 12 October 2022

Published: 18 October 2022

Publisher's Note: MDPI stays neutral with regard to jurisdictional claims in published maps and institutional affiliations.



Copyright: © 2022 by the authors. Licensee MDPI, Basel, Switzerland. This article is an open access article distributed under the terms and conditions of the Creative Commons Attribution (CC BY) license (<https://creativecommons.org/licenses/by/4.0/>).

1. Introduction

In recent years, sustainable automotive design has gained progressive interest, namely regarding the design of automotives with a lightweight structure and efficient fuel economy to tackle environmental issues. Small lightweight electric vehicles, such as an electric heavy quadricycle categorized by the EU as an L7e vehicle, is an alternative that could deliver a solution in traffic mitigation for the future urban individual mobility with limited space conditions [1–3]. Motorized quadricycles also offer a lower carbon footprint and high energy consumption efficiency in the battery mass to total vehicle mass ratio [4]. Nonetheless, regulations for L7e vehicle registration require considerably less strict safety standards [5]. Thus, the quadricycles typically do not offer passengers the same passive safety system as larger passenger car models. Several researchers have worked on the structural design to the improve occupant safety of quadricycles under collisions with fixed objects [6–8] as well as car-to-car collisions with other larger vehicles on the road [9–11]. However, the car-to-car crash evaluation is rather complicated, owing to the diversity of the combinations of vehicle models and collision conditions [12]. Studies on quadricycle-involved car-to-car crashes are thus limited.

Zeng et al. [13] empirically studied the injury degree of drivers in the car-to-car crash dataset. The study showed that newer vehicle models and lower speed ratios are related to the lower injury severity of both drivers. Moreover, head-on crashes were significantly more severe than oblique and rear-ended crashes and are considered one of the deadliest car accidents. Huang et al. [14] investigated the crashworthiness and crash-aggressivity in accidents between different vehicle types, and the dominating effect of vehicle mass was identified. Thompson et al. [15] analyzed the accident database and reported a strong trend of driver injury with an increasing mass ratio. The drivers of the lighter car were more prone to sustain more severe injury than the drivers of the heavier car. Additionally, poor structural interactions in a frontal car-to-car collisions can increase the injury probability of occupants with a high overlap due to compartment deceleration pulse and a low overlap due to intrusion. According to the frontal injury statistics and previous research [16–18], the thorax, head, and neck have been listed as the primary body parts injured.

Determining the crash compatibility between L7e vehicles and other vehicles can be challenging due to the mass difference and the relatively short crumple zone of the L7e vehicle. Kolke et al. [19] studied crash compatibility between sport utility vehicles (SUVs) and minicars by conducting an offset-frontal crash test. The results showed that although both cars offered high occupant protection from the individual crash test, the occupants in the minicar experienced more severe injury than the occupants in the SUV. Sadeghipour et al. [20] proposed safety priorities for microcars: the restraint system, compartment strength, and structural interaction. The frontal crash compatibility assessment approach using a mobile deformable barrier was also developed and verified via finite element simulation.

The European New Car Assessment Programme (Euro NCAP) has recently introduced a mobile progressive deformable barrier (MPDB) to represent car-to-car collisions [21]. However, several researchers have proposed that the MPDB test should account for the vehicle's size and mass [10,22,23]. Zhendong et al. [24] combined statistical analysis of different MPDB test data and suggested that collision compatibility can be improved by modifying the front structure load transmission path and energy dissipation. Several studies proved that the vertical alignment of longitudinal members or the involved vehicles' primary energy-absorbing structure (PEAS) was the key to preventing override or underride in head-on crashes [25,26]. Yonezawa et al. [27] found that vertical alignment mismatches of more than 100 mm can cause the override/underride of the opponent vehicles. The underride car might experience more damage than the override car. When a smaller car, such as a microcar or a heavy quadricycle, crashes into a larger vehicle, it is anticipated to experience more severe damage and occupant injury than when tested with a rigid wall crash test. However, minimal work has investigated the influence of incompatibility in both the mass and PEAS alignment of microcar crash tests.

The L7e vehicle presents a lack of passenger safety because of its smaller dimensions and lighter weight than the opponent vehicles. It also causes the crash incompatibility problem when the collision occurs. Thus, the objective of the current study is to examine the L7e vehicle's frontal crash behaviors and the severity of the crash under rigid-wall and car-to-car crash scenarios. Parameters including impact velocity, the size of the opponent car, and the vertical alignment of the primary energy-absorbing structure were investigated based on the criteria in line with the Euro NCAP assessment protocol. The crash simulation was conducted via LS-DYNA finite element analyses, and the occupant injury of the hybrid III 50th percentile male dummy was assessed. Characteristics of the structural interaction and occupant injury severity were evaluated and compared in terms of the deformation of the front structure, energy absorption distribution, intrusion of the vehicle compartment, and biomechanical forces of the occupant dummy.

2. Materials and Methods

The finite element models of the opponent vehicles used in the current study (2010 Toyota Yaris sedan and 1997 Toyota Rav4 SUV) were developed by the National Crash Analysis Center [28,29]. The models were validated through the Roadside Safety Verification

and Validation Program (RSVVP), an analytical tool to statistically quantify the consistency between the simulation and test results suggested by [30]. Appendix A shows result comparisons of the rigid wall crashes from the current FE simulations with experimental results from Fischer [31]. A validation of the hybrid III 50th percentile male dummy based on the frontal sled test performed by Eggers and Adolph [16] is also explained in Appendix A.

This section describes the L7e FE model employed to examine the crash compatibility and occupant injury with different crash scenarios and various bumper heights to evaluate the overall performance of the L7e structure under the frontal crash.

2.1. Electric Heavy Quadricycle Finite Element Model

The electric heavy quadricycle, categorized by The United Nations Economic Commission for Europe (UNECE) as an L7e vehicle, is defined as a three- or four-wheeled motor vehicle for carrying passengers or goods with an engine power that does not exceed 15 kW. In the case of the carrying-passenger vehicle, the structural weight should not exceed 450 kg, excluding the mass of the battery, and the maximum designed load for the passenger is 200 kg. The current study uses the Smart Fortwo structure as an L7e vehicle reference. The overall dimensions of the structure were 1.4 m in width, 2.5 m in length, and 1.5 m in height, with an overall structural weight of the vehicle equal to 375 kg. The finite element model was created using 4-node Belytschko shell elements consisting of 117,215 nodes and 118,058 elements with the components as shown in Figure 1. The thickness of each component was assigned as listed in Table 1. Five components of the frontal structure, including the upper beam, front rail, bumper, crash box, and subframe, were examined for passenger protection during a crash accident of the L7e vehicle. The material properties of the DP600 were assigned to the whole structure, except the crash box, bumper, and front rail, which were defined by Al-6061 [32].

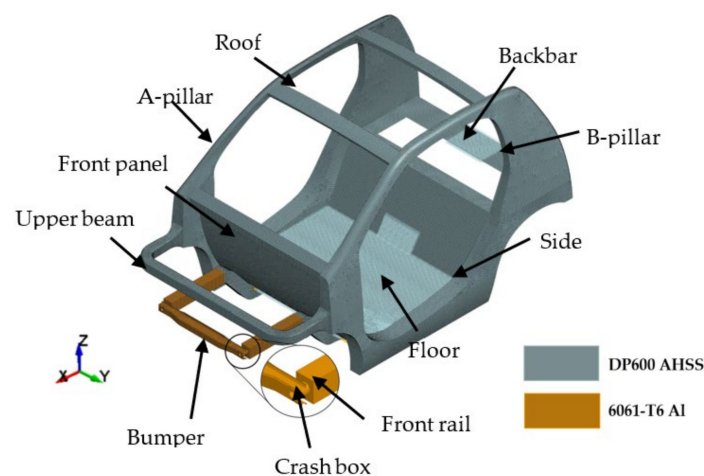


Figure 1. Structural components of the L7e vehicle finite element model.

Table 1. The thickness of each structural component.

Sections	Components	Thickness
Frontal Structure	Bumper	2.0 mm
	Upper beam	1.2 mm
	Front rail	
	Crash box	
	Subframe	
Passenger Compartment	Backbar	3.0 mm
	Pillars	2.0 mm
	Roof	
	Floor	
	Side beams	

The wheel systems were linked to the car body using the Constrained Nodal Rigid Body (CNRB) option in LS-DYNA, which allows the application of angular velocity around the wheel axles. The hybrid III 50th percentile male dummy driver [33] was added to the model to investigate the occupant's injury during a crash accident. The `CONSTRAINED_RIGID_BODY` connects a driver's seat to the floor structure. The restraint system comprising a buckle, anchor, retractor, and D-ring were also included. The seatbelt pretensioner was set to fire at 10 ms after impact with a 65 mm seatbelt pulled in [34] and the load limit of 6 kN. Mass elements were applied to distribute the weight of the non-structural components, i.e., 275 kg battery on the floor structure and 65 kg motor and other driving systems on the back bar structure. The total weight of the complete L7e model was 790 kg, including a 715 kg vehicle weight and 75 kg dummy weight.

2.2. Crash Scenarios

The structural performances of the L7e model, such as the deformation and energy absorption of each component, were investigated based on four cases of frontal crash accidents. The scenarios included a full-frontal crash with the rigid wall, a 50% offset crash with the rigid wall, a full car-to-car collision, and a 50% offset car-to-car collision. For the impact with the rigid wall cases, the condition from Euro NCAP was employed, as illustrated in Figure 2, with various initial velocities from 30 to 90 kph. Contact interactions between all the structural parts of the car and the rigid wall were assigned using `CONTACT_AUTOMATIC_SINGLE_SURFACE` by specifying static and dynamic friction coefficients of 0.2 and 0.1, respectively.

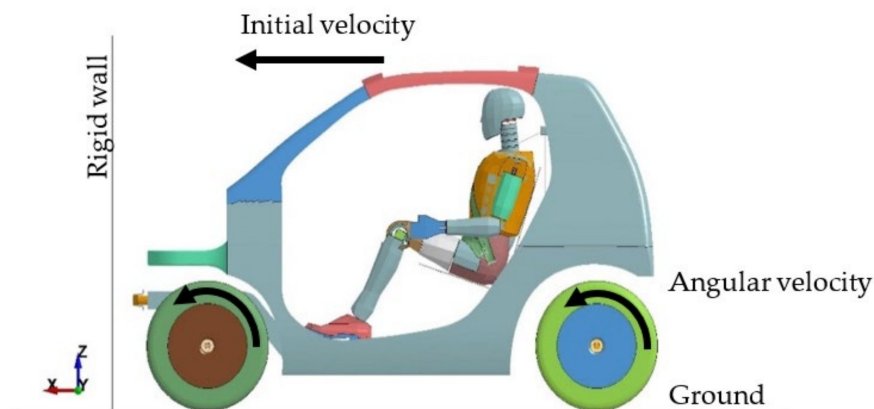


Figure 2. The initial condition and model set-up for the rigid wall crash scenario.

In the cases of car-to-car collisions of the L7e vehicle with larger opponent vehicles, the crash simulation of Toyota Yaris and Toyota Rav4 models from NCAC were studied. These models were selected as representatives of the commercial passenger car platforms for a sedan and SUV, while the FE models were previously validated by NCAC [28,29]. The centerlines of the vehicles in the longitudinal plane were used to identify the full-frontal and offset-frontal crash accidents, as shown in Figure 3. In the full-frontal crash, the centerlines of the two vehicles were aligned, and the initial velocities of the cars were in an opposed direction (Figure 3a). For a 50% offset-frontal crash, the opponent car crashed against the half width of the frontal structure of the L7e model (Figure 3b). The boundary conditions were defined similarly to the impact analysis with the rigid wall. At the same time, the contact surfaces of the two vehicles were assigned using `AUTOMATIC_SURFACE_TO_SURFACE` contact with a friction coefficient of 0.2.

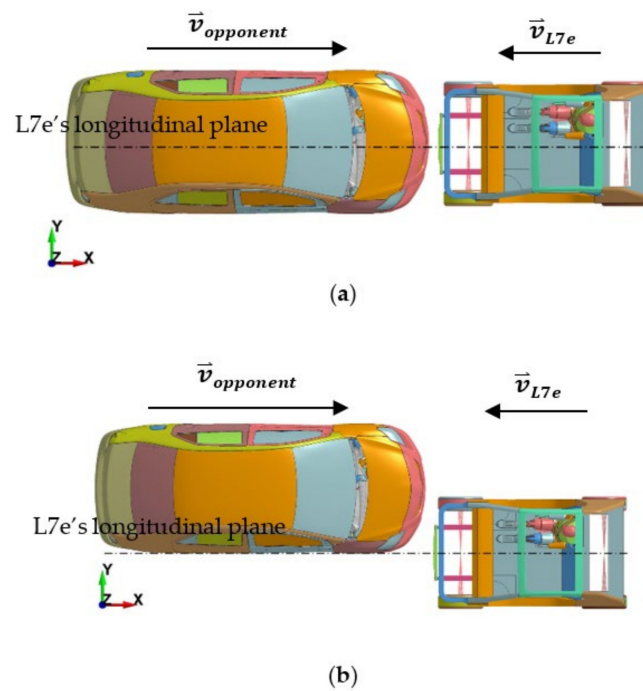


Figure 3. Vehicle positions for crash scenarios: (a) full-frontal; (b) 50% offset-frontal.

The effects of adjusting the bumper height of the L7e vehicle on the crash compatibility and injury severity of the L7e vehicle’s driver under the frontal crash accident were then examined. The part 581 zone [35] was employed to classify the bumper height of the L7e model. This zone typically defines the range of the bumper height from 16–20 inches (407–507 mm) measured vertically from the ground to the centerline of the bumper to ensure that the vehicles have a common interaction alignment of the absorbing structure. Furthermore, the 581 zone requires that the primary energy-absorbing structure (PEAS) overlap with at least 50% of the secondary energy-absorbing structure (SEAS) connecting with the primary structure. The L7e vehicle’s bumper heights in three cases of 382 mm, 495 mm, and 532 mm—corresponding as low, medium (preliminary model), and high—were studied for the interaction effects with different opponent vehicles (Figure 4).

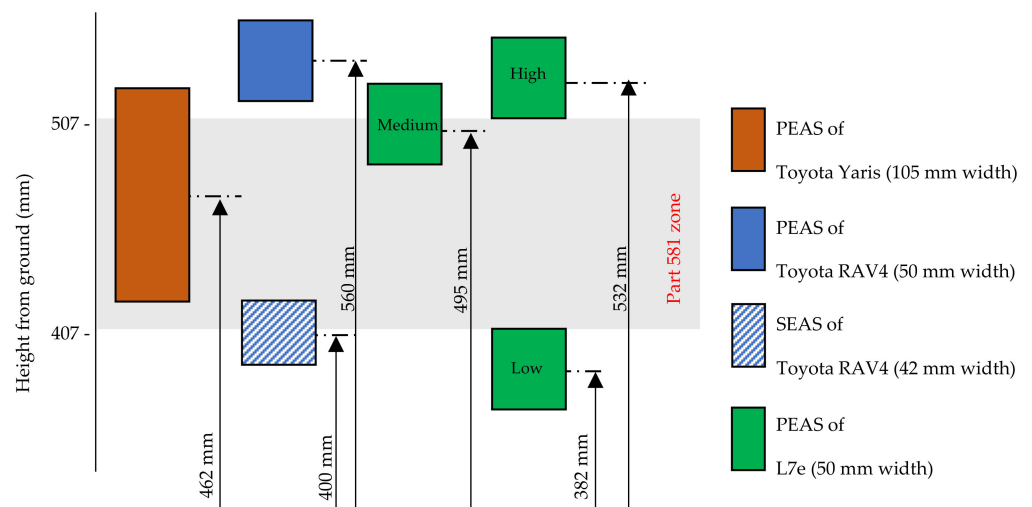


Figure 4. Ranges of the bumper height for the L7e model according to the part 581 zone regulation.

3. Structural Performance Evaluation from Crash Analysis

This section provides results from the structural analysis of the L7e model under different crash scenarios. The concept of residual space is also proposed as a preliminary criterion of safety assessment in car-to-car crash accidents.

3.1. Frontal Impact of L7e Vehicle with Rigid Wall

The L7e model was analyzed with a full-frontal and 50% offset-frontal crash with a rigid wall. The effects of the initial crash velocity were primarily examined to clarify the structural characteristics and energy-absorption performances under low- and high-impact speeds (Figure 5). The low initial velocity was assigned at 30 kph, and the high impact speeds varied from 50 kph to 90 kph. It can be seen that the high impact speeds caused both the rigid wall force and energy absorption to be higher than the low initial velocity, and the maximum rigid wall force and the energy absorption of the L7e model increased due to extensive deformation. The energy absorption at high impact speeds severely accrued around three and five times when the initial velocity increased from 50 kph to 70 kph and 90 kph, respectively, while the maximum rigid wall forces were slightly different. Thus, frontal structures are the essential components to design to absorb the impact energy and prevent occupant injury from the remaining energy during a crash accident.

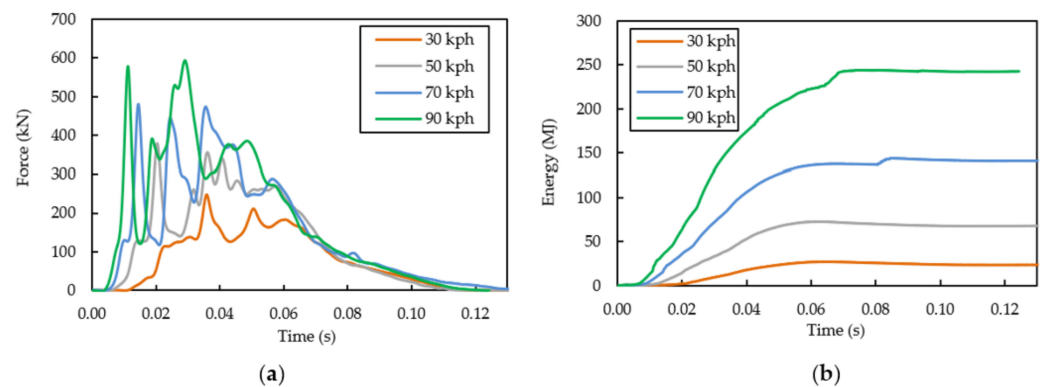


Figure 5. Time histories of rigid wall force and absorbed energy of L7e model during a frontal crash: (a) rigid wall force; (b) energy absorption.

In the cases of full-frontal impact, regardless of the initial crash speed, both the PEAS and SEAS were fully deformed (Figure 6a). In contrast, only the impact side of the front structure was deformed under the 50% offset-frontal crash (Figure 6b). The final deformation of the frontal structures also increased when the initial crash velocity increased. The upper beam and front rail of the L7e vehicle were collapsed in buckling mode and absorbed most of the crash energy in all cases.

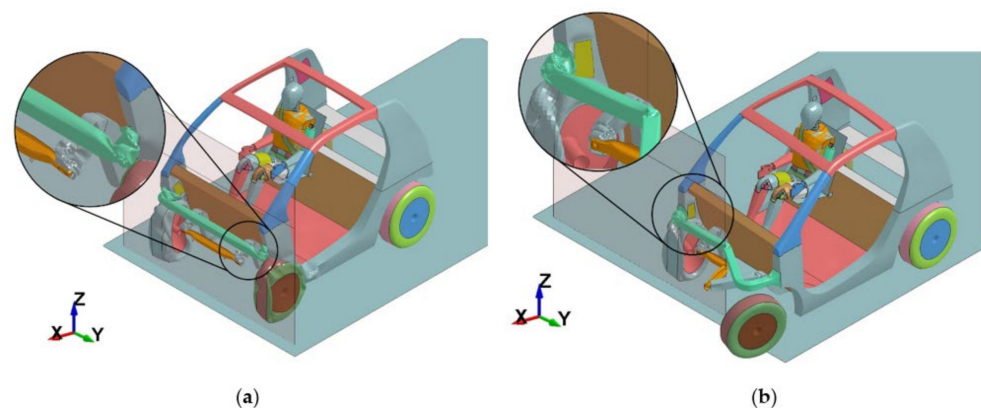


Figure 6. Deformation patterns of L7e vehicle structure under 50 kph collision with a rigid wall: (a) full-frontal crash; (b) 50% offset-frontal crash.

The energy absorption (EA) of the frontal structure for each impact velocity is compared in Figure 7. The front structure tended to absorb higher energy when the impact velocity was low, in which case the minor deformation of the passenger compartment was observed. In addition, the EA of the front structure for the offset frontal crash was slightly higher than that of the full-frontal crash for all initial impact velocities. The highest percentage of the front structure's EA occurred when the impact velocity was 30 kph for both cases, absorbing 58.3% and 71.5% of the crash energy during the full-frontal and offset-frontal crashes, respectively. The front structure's EA dropped from 17% to 35% when the impact speed reached 50 kph, showing the front structure's significance under low-velocity crashes. At higher impact speeds, the deformation patterns and EA percentage were similar to the 50 kph crash. Therefore, the low- and high-impact speeds were well represented by 30 kph and 50 kph, respectively. It was observed that there was no significant difference between the EA of the frontal structure for crashes with the rigid wall when the L7e vehicle's bumper height was changed because both the PEAS and SEAS were entirely in contact with the rigid wall irrespective of their heights.

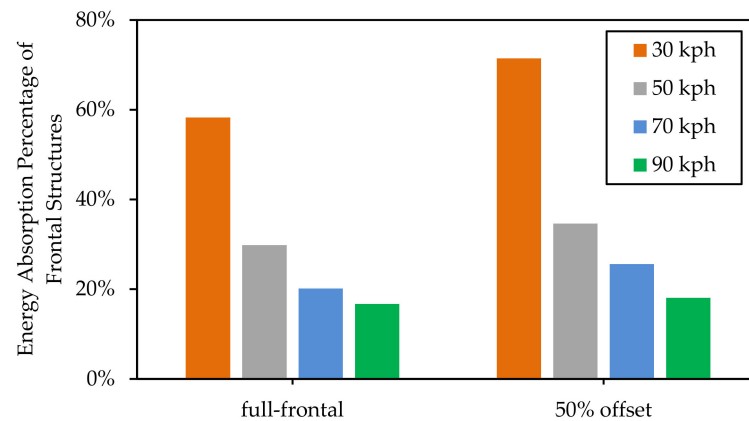


Figure 7. Energy absorption of the frontal structure from impact with a rigid wall.

3.2. Full-Frontal Car-to-Car Collision

The full-frontal car-to-car collisions of the L7e model were performed by crashing with a sedan and an SUV model, with the initial impact speeds for both vehicles being 30 kph and 50 kph. The simulation of the car-to-car collision was verified and validated by comparing the FE results with the theoretical analysis, the so-called "Routh method," as described in Appendix B. This procedure had been successfully implemented by Kisilowski et al. [36] to determine and investigate the impulse forces during the crash and post-crash velocities. Results comparisons showed the fair agreement of the impulses and after-crash angular velocity vectors between the simulation and the Routh method. Figure 8 compares the impact energy absorbed by the preliminary model of the L7e vehicle with a medium bumper height when crashing into the rigid wall and another opponent vehicle. The absorbed energy in rigid-wall crash tests was noticeably less than that in the case of car-to-car collisions for both the sedan and SUV, especially at a higher impact speed. These results suggest that the impact test with the rigid wall can underestimate the severity of car-to-car crash accidents.

An example of the FE results from a collision with the Toyota Yaris sedan at 50 kph is displayed in Figure 9a. In this case, the front rail, subframe, and upper beam were principally deformed and absorbed the crash energy similar to the collision with the rigid wall (Figure 9b). However, the deformation modes of the front rail and subframe differed from the former case with the rigid wall depending on the L7e vehicle's bumper height since the PEAS was not entirely in contact with the opponent vehicle's mainframe during the crash.

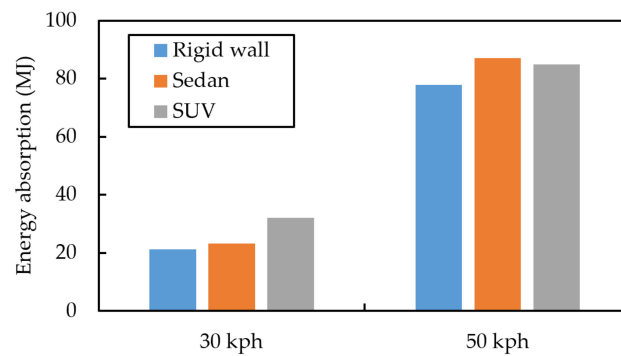


Figure 8. The absorbed energy of L7e vehicle in frontal crashes with the rigid wall and another opponent vehicle.



Figure 9. Full-frontal impact collision between the L7e vehicle and sedan: (a) vehicle deformations during the crash; (b) the deformed shape of the upper beam after the crash.

The deformed shapes of the frontal structure can be categorized into three modes, i.e., bending, buckling, and combined modes (Figure 10). Different modes were detected in the L7e vehicle during frontal crashes depending primarily on the initial impact points of the front rail and the positions of the PEAS and SEAS of the opponent models (Figure 11).

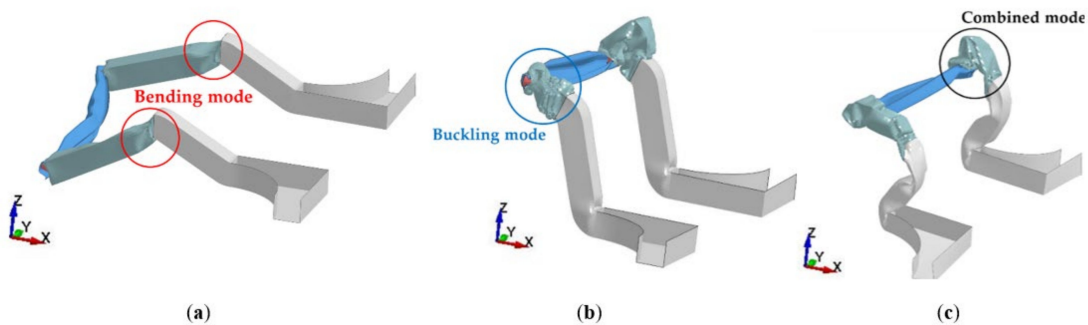


Figure 10. Front rail deformation: (a) bending mode; (b) buckling mode; (c) combined mode.

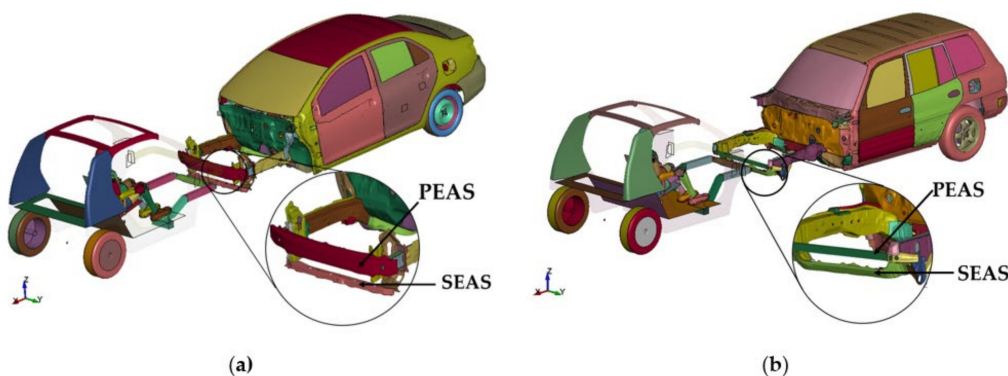
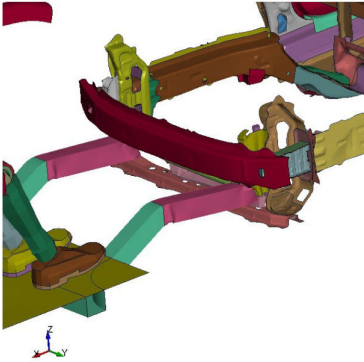
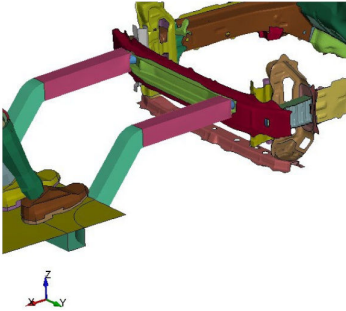
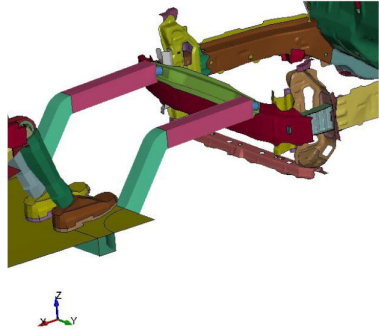
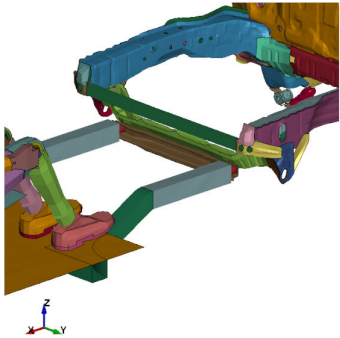
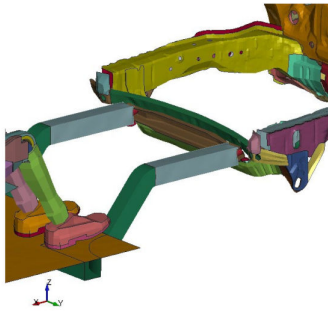
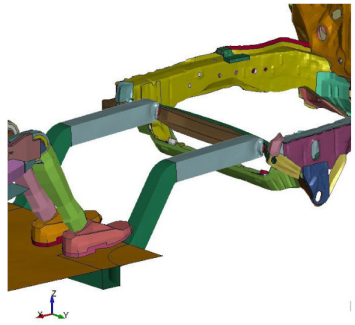


Figure 11. Positions of the PEAS and SEAS: (a) sedan model; (b) SUV model.

Table 2 shows the impact locations with the sedan and the SUV for different L7e vehicle's bumper heights. The energy absorption of the frontal structures and the deformed shape of the front rail under full-frontal car-to-car collision with different initial crash velocities are summarized in Table 3. It can be noticed that the EA percentage of the upper beam was around 20–30% in the low-velocity crash; meanwhile, in the high-velocity crash, the upper beam had an EA percentage of only 9–12%. Hence, the upper beam played an important role in the low-velocity crash. The different EA percentages of the upper beam in the low-velocity crash also depended on the bumper height, in which the low bumper height absorbed the highest impact energy. Additionally, the bumper height correlated with the deformation shape of the front rail under the crash. Thus, the EA of the front structure was closely related to the front rail's deformed shapes.

Table 2. The positions of L7e vehicle's bumper height and the opponent vehicle's PEAS and SEAS.

Opponent Vehicle	Bumper Height		
	Low	Medium	High
Sedan			
SUV			

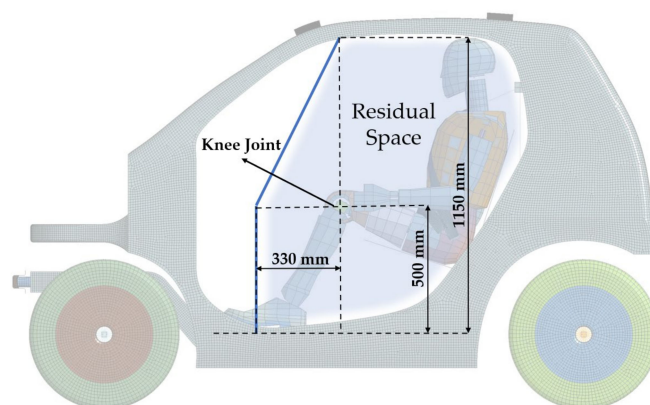
The low bumper height of the L7e vehicle did not fully interact with the front structure of the opponent vehicles for both the sedan and SUV models. When the L7e vehicle and sedan crashed, the L7e vehicle's bumper impacted the sedan's radiator and engine instead of the PEAS. However, the rigidity of those components created a buckling of the front rail. The buckling mode of the front rail distinctively showed high energy absorption, especially at the low-impact speed, resulting in lower energy dissipating to the passenger compartment. On the contrary, the mismatch of the L7e vehicle's bumper height and the SUV's PEAS caused an underride of the L7e vehicle. Thus, the bending effect governed the L7e vehicle's front rail deformation.

Table 3. Results of full-frontal car-to-car crash analysis of the L7e model.

Opponent Vehicle	Initial Velocity	Bumper Height	Energy Absorption (%)				Deformed Mode of Front Rail
			Front Rail	Subframe	Upper Beam	Total	
Sedan	30 kph	Low	37.0	0.64	30.0	67.6	Buckling
		Medium	22.3	15.4	23.9	61.6	Combined
		High	19.4	18.9	24.7	63.1	Combined
	50 kph	Low	20.3	4.46	10.1	34.9	Buckling
		Medium	9.38	14.3	11.3	34.9	Combined
		High	9.05	14.6	11.5	35.2	Combined
SUV	30 kph	Low	11.8	1.06	29.1	41.9	Bending
		Medium	32.5	8.55	21.6	62.7	Buckling
		High	33.9	7.38	20.1	61.3	Buckling
	50 kph	Low	9.42	9.99	11.2	30.6	Bending
		Medium	13.6	6.82	10.3	30.7	Buckling
		High	11.1	6.09	9.50	26.7	Buckling

The L7e vehicle's medium bumper height was located at the exact position of the sedan's PEAS and between the positions of the PEAS and SEAS of the SUV. Therefore, the structures could interact appropriately in frontal crashes and absorb the impact energy. The combined buckling and bending mode of the front rail occurred when impacted by the sedan, while the buckling mode of the front rail was noticed when impacted by the SUV. Thus, this design generated the highest front rail EA percentage when impacted by the SUV. For the high L7e vehicle's bumper height, the vertical alignment was somewhat mismatched with the sedan's bumper but utterly compatible with the SUV bumper's height. Thus, the deformations of the front rail after the crash were in combined mode and buckling mode for the former and latter cases, respectively.

Vehicle deformations can be preliminarily used to assess the safety of the occupants in a crash. A residual space is proposed to represent the safety zone of the passenger in the L7e vehicle based on the position of the Hybrid III 50th percentile male dummy to evaluate occupant safety during the crash accident (Figure 12). The knee joint position was defined as the reference point to identify the safety zone. The front threshold of the residual space was projected at 330 mm from the knee joint to the front area. The upper threshold was defined according to the dummy height in the sitting position at 1150 mm high. The occupant safety of the L7e model was certified if none of the structural parts of the vehicle intruded into the residual space during the crash.

**Figure 12.** Proposed residual space for the L7e model.

The results showed that the compartment zone was slightly deformed when the initial velocity of 30 kph was assigned, and none of the structural parts of the L7e vehicle intruded into the residual space. A large deformation of the frontal structure occurred with the

car-to-car crash speed of 50 kph. The car was mainly deformed at the front panel, A-pillar, and side structures. When crashing with the sedan, the deformation of the L7e structure did not intrude into the residual space, where the maximum and minimum clearances of 75 mm and 14 mm were found at the high and low bumper height, respectively (Figure 13a). However, the frontal parts intruded into the residual space for 30 mm (indicated by the negative clearance in Table 4) when the low-bumper L7e vehicle crashed with the SUV, where the L7e vehicle underrotated the SUV as mentioned earlier. The medium- and high-bumper heights were safe (Figure 13b). Thus, only the crash with the bending mode of the front rail caused an intrusion into the residual space of the L7e vehicle. It is also worth noting that the deformation of the frontal structure was apparently more severe in the case of car-to-car crashes than in the case of the rigid-wall crash because the head-on collision had more impact energy from the opponent vehicles than the car-to-rigid wall crash. Additionally, full contact with the rigid wall had more advantages in energy dissipation to other parts of the vehicle than partial contact with the opponent vehicle, which resulted in a smaller deformation. Therefore, the intrusion from the car-to-rigid wall was smaller than the car-to-car collisions.

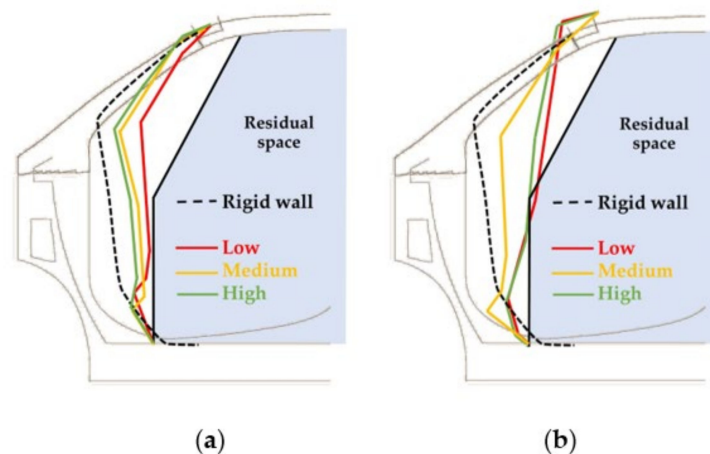


Figure 13. Structural deformation of L7e vehicle during the full-frontal car-to-car collisions at 50 kph crash speed: (a) crashing with the sedan; (b) crashing with the SUV.

Table 4. Minimum clearance to residual space for different crash scenarios.

Opponent Vehicle		Sedan			SUV		
		Low	Medium	High	Low	Medium	High
Minimum clearance to residual space (mm) *	50 kph (F)	+14	+63	+75	−30	+85	0
	50 kph (OL)	0	−25	−55	−191	−223	−236
	50 kph (OR)	+240	+240	+240	+240	+240	+240

* Positive values indicate clearance between L7e vehicle structural parts and residual space, while negative values indicate intrusion into the residual space.

All analyses showed that the geometry of the front structure of the vehicle parties essentially affected the crash compatibility in the car-to-car collision. Compatible bumper heights provided the buckling mode of the front rail during the crash. The energy absorption was well distributed among the front rail and the upper beam for both low and high-impact velocities. Thus, no intrusion into the residual space occurred in such cases. The most effective position of the bumper for the L7e vehicle was the high level in which the energy absorption was the highest, and the maximum clearance to the residual space was found. In addition, the frontal structure of the L7e vehicle tended to absorb a higher impact energy in the car-to-car crash than in the collision with a rigid wall, owing to the lighter mass of the L7e vehicle compared with the opponent vehicle. Hence, the design

of L7e vehicle safety based on a crash test with a rigid wall did not represent a real-life accident well and underestimated the severity of the car crash.

3.3. 50% Offset-Frontal Car-to-Car Collision

For the 50% offset-frontal car-to-car collisions with different L7e vehicle bumper heights, the simulation results were different from the full-frontal crash due to unsymmetrical deformations. Table 4 compares the minimum clearance of the structural part with the residual space in all the car-to-car crash scenarios. Note that the clearance was equal to zero when the deformed frontal structure was precisely at the residual space's threshold. Positive clearances suggested no intrusion of the L7e vehicle structure to the residual space, in which the clearance of the undeformed frontal structure was +240 mm. Negative clearances specified the intrusion of a structural component into the residual space. The letters F, OL, and OR in the parentheses denote the full-frontal crash and 50% offset crash when the clearance was measured on the car's left (near) side and the crash's right (far) side, respectively.

For the cases with a 50 kph initial crash velocity, it was found that the offset crashes resulted in a more severe deformation on the near-crash side (OL) than in the case of a full-frontal collision (F), with the more extensive intrusion of the L7e vehicle's residual space. Thus, the occupant safety based on the assigned residual space was not satisfied. However, no deformation occurred to the passenger compartment's far-crash side (OR), indicated by the clearance of +240 mm. In the 30 kph cases, the passenger compartment was not deformed in all of the recorded locations at the initial velocity of 30 kph. Moreover, horizontal alignment was another significant factor affecting compatibility for offset crashes. Although the medium bumper height was in a proper vertical alignment, the bumper only partially impacted the other party due to horizontal misalignment, as shown in Figure 14. The horizontal overlap between the L7e vehicle and the sedan and SUV was only 16.8% and 4.6%, respectively, and caused the front rail to bend to the side and absorb less energy than expected. Thus, for small cars such as L7e vehicles, the horizontal alignment of the bumper is also necessary to increase the overlap areas of the SEAS between the two opposing cars to mitigate crash severity. Recommendations on the minimum horizontal alignment should be further investigated.

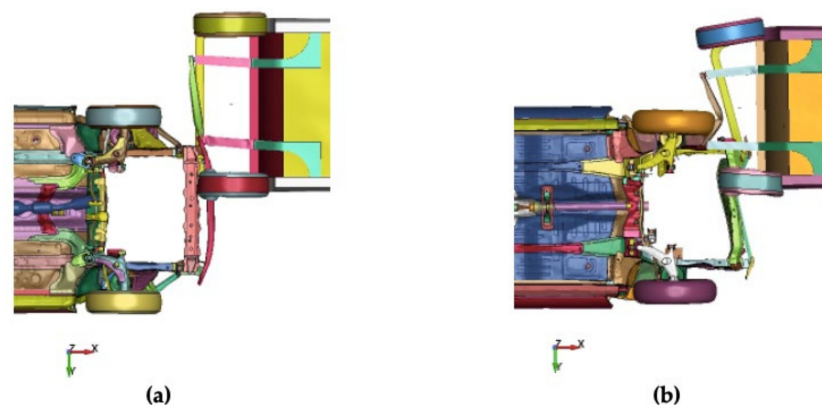


Figure 14. Offset-crash configurations for L7e vehicle with medium height bumper: (a) L7e vehicle and sedan; (b) L7e vehicle and SUV.

It is also worth noting that, in the case of medium and low bumper heights, the L7e vehicle bumper was not at all in contact with the PEAS and SEAS components of the SUV. However, the bumper was in complete contact with the SUV tire, and the front rail absorbed relatively high energy (Figure 15). In addition, the SUV tire directly contacted the front panel and caused a large deformation due to the vertical misalignment of the high bumper height. This crash scenario could also initiate occupant injuries due to the high impact forces transferred to the occupants.

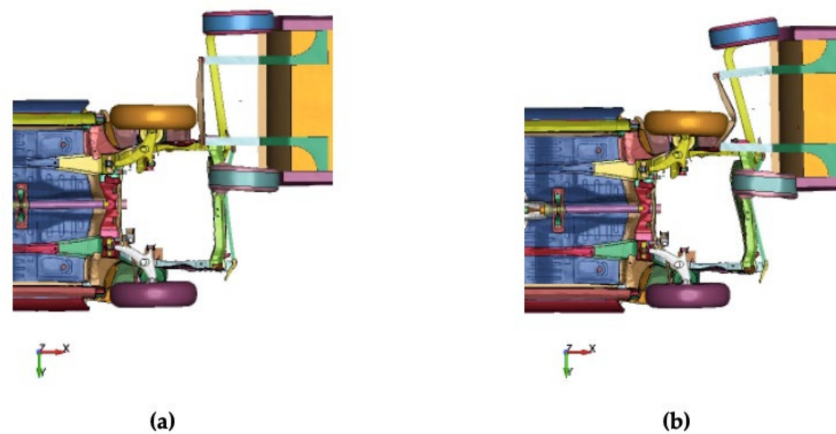


Figure 15. Crash configurations of L7e vehicle and SUV at low bumper height: (a) impact position of bumpers; (b) bumper deformation.

4. Occupant Injury Assessment from Crash Analyses

A crash accident can cause impact damage to vehicle structures and injury to the occupant's body parts. Structural deformation is commonly used to assess a vehicle's safety, whereas passenger safety might not directly correspond to the structural response. Thus, an occupant injury assessment was employed to estimate the level of personal injury from the crash accidents for each body part due to direct or indirect impact loading. This section describes the injury assessment of the L7e vehicle occupant based on the AIS 2+ probability of the hybrid III 50th percentile male dummy. The injury severities are then compared with structural deformations and intrusions into the residual space. The head, neck, and femur injuries were focused on when examining the results.

4.1. Occupant Injury Assessment

The occupant injuries common in frontal accidents are head, neck, femur, and thorax injuries. The parameters used in the current study to assess injury severity at these parts were the Head Injury Criterion (HIC), Neck Injury Criterion (N_{ij}), femur axial force, and chest deflection. Both the femur axial force and chest deflection can be directly evaluated from the dummy deflection, while the HIC and N_{ij} are calculated from acceleration and body forces, respectively.

The HIC was first recognized by the National Highway Traffic Safety Administration (NHTSA) to determine the head injury threshold using a head acceleration–time profile [35]. The HIC can be calculated from the three-dimensional acceleration magnitude during the head impact [36] with:

$$HIC_{15} = \max \left[\frac{1}{t_2 - t_1} \int_{t_1}^{t_2} a(t) dt \right]^{2.5} (t_2 - t_1) \quad (1)$$

where $a(t)$ is the resultant acceleration at the head's center of gravity and t_2 and t_1 are the time intervals of the maximum head acceleration during an impact accident. A time interval of 15 or 36 ms is usually used. The calculation of the N_{ij} involves a combination of axial force (F_z) and sagittal moment (M_y) at the occipital condyle by normalizing with the critical axial force (F_{int}) and critical sagittal moment (M_{int}), and is expressed by [36]:

$$N_{ij} = \frac{F_z}{F_{int}} + \frac{M_y}{M_{int}} \quad (2)$$

For the hybrid III 50th percentile male dummy, the intercept value of the critical axial force was 5440 N for both tension and compression, while the critical sagittal moment was 415 N·m and 166 N·m for flexion and extension, respectively. The axial force and sagittal moment were paired into four cases: tension–flexion, tension–extension, compression–

flexion, and compression–extension, to evaluate the maximum value among these four cases as the N_{ij} value.

The Association for the Advancement of Automotive Medicine proposed a coding system called the Abbreviated Injury Scale (AIS) to classify and describe the anatomical severity of trauma by scaling from one (minimal) to six (maximal) [37,38]. Moderate injury, classified by level 2 of the AIS (AIS 2+), is always the criteria for preliminary injury assessment during crash simulations [39]. The AIS 2+ represents the occupant injury as a skull fracture at the head, minor compression fracture of the cervical spine at the neck, a sternum or 2–3 rib fracture at the chest, and a femoral muscle laceration at the femur. The probability calculations of occupant injuries according to the AIS 2+ at the head, neck, and femur have been developed in a mathematical model of the injury risk by fitting the injury criteria data to the occupant injury data [40]. For the head injury, the probability of occupant injury is calculated by determining the probability from Equation (3) with the bell-shaped probability density function in Equation (4), where $P(x_i)$ is the skull fracture probability and $P(x)$ is a probability distribution function with μ equal to 6.9352 and σ equal to 0.84664. The cervical spine fracture probability, $P(N_{ij})$, and the femoral muscle laceration probability, $P(F_{ax})$, are also calculated by a fitted logistic regression model as shown in Equations (5) and (6), respectively.

$$P(\ln(HIC_{15})) = \int_0^{\ln(HIC_{15})} P(x) dx \quad (3)$$

$$P(x) = \frac{1}{\sigma\sqrt{2\pi}} e^{\left(\frac{-(x-\mu)^2}{2\sigma^2}\right)} \quad (4)$$

$$P(N_{ij}) = \left(1 + e^{5.2535 - 4.1(N_{ij})}\right)^{-1} \quad (5)$$

$$P(F_{ax}) = \left(1 + e^{5.795 - 0.5196(F_{ax})}\right)^{-1} \quad (6)$$

The neck injury criteria (N_{ij}) value is determined by using Equation (2) and F_{ax} is the femur axial force from the femur load cell.

4.2. Dummy Responses in Frontal-Impact with Rigid Wall

The preliminary model of the L7e vehicle with a medium bumper height was employed to study the occupant kinematics and probability of severe occupant injuries under a frontal crash with the rigid wall. The time histories of head acceleration, neck axial force and moment, and femur forces for various initial velocities are illustrated in Figure 16. It can be seen that the high head acceleration, neck axial force, and neck moment occurred at a similar time instance at about 60–100 ms after the crash when the shoulder belt retracted the dummy's upper body due to the retractor payout limit. The femur forces occurred earlier because a lap belt restrained the lumbar due to the friction at the slip ring. After that, the femur was still moving forward due to its inertia. At the beginning of the crash events, the dummy's neck moved in an extension posture, indicated by positive neck moments. Though, for the high initial crash velocities, such as 70 kph, the neck flexion specified by negative moments obviously occurred afterward due to the head's inertia when the safety belt restrained the movement of the dummy's body. The injury severity for a full-frontal crash was higher when the initial impact velocity increased where the head and neck injuries were mainly affected (Figure 17a). At the low-speed impact of less than 50 kph, the occupant injury was minimal, corresponding to the substantial energy absorption of the frontal structure and the minor deformation of the passenger compartment. For the impact velocity of 70 kph and higher, the probability of severe injury to the head, neck, and femur ranged from 20 to 100%, which means that the occupant's safety was highly compromised.

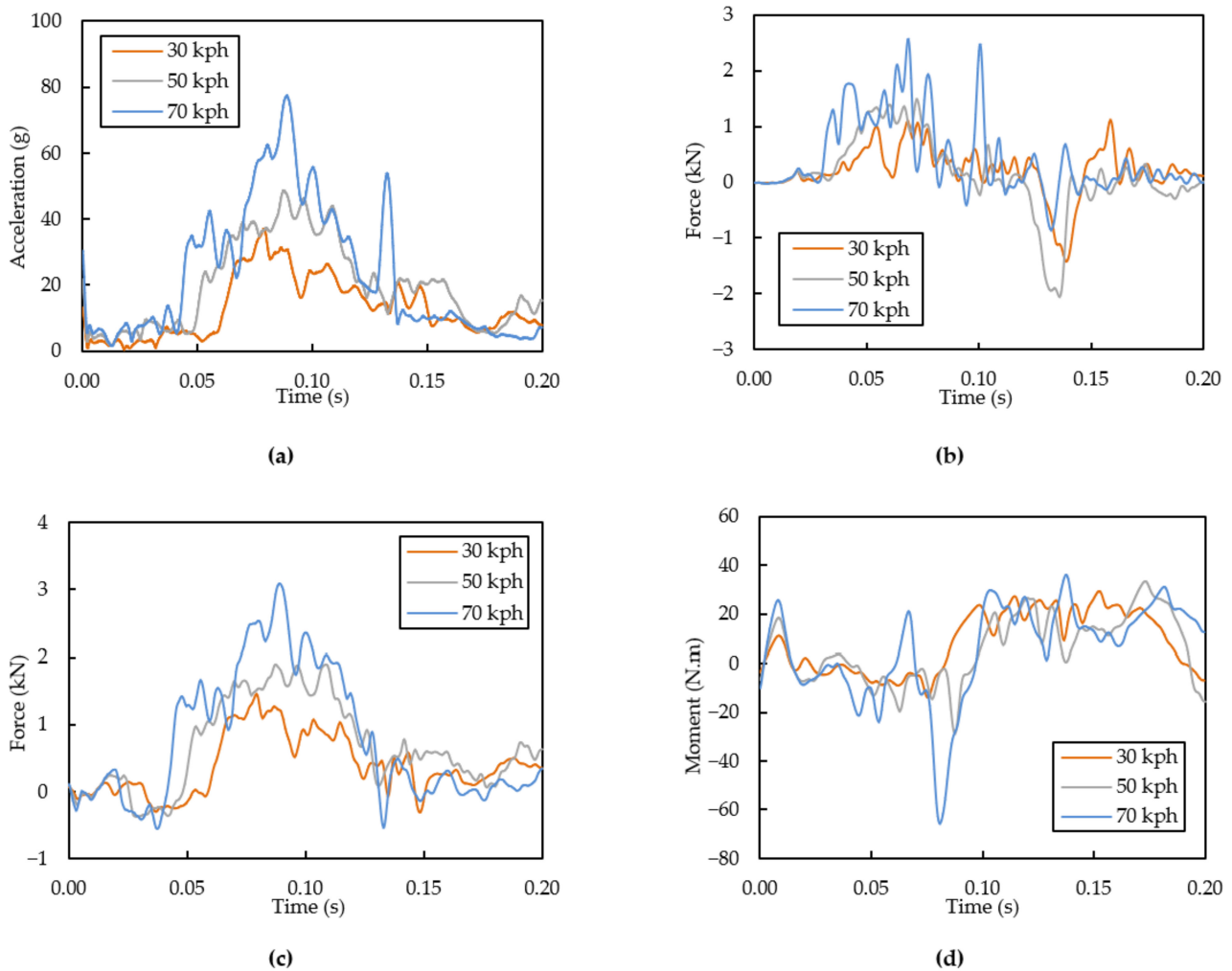


Figure 16. Time histories for the full-frontal crash with a rigid wall: (a) head acceleration; (b) femur forces; (c) neck axial forces; (d) neck axial moments.

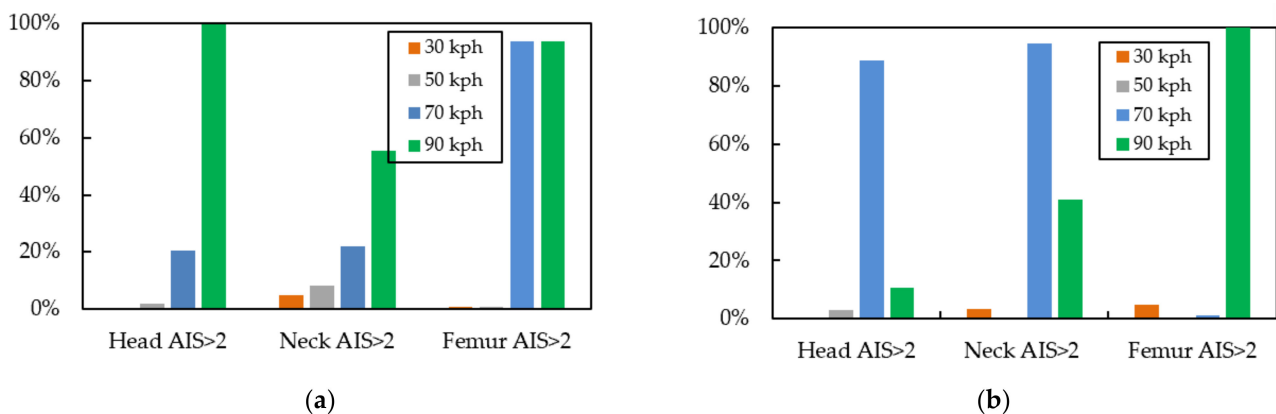


Figure 17. Probability of occupant injury from rigid wall crash analyses: (a) full-frontal impact; (b) 50% offset impact.

The results from the offset impact (Figure 17b) showed that the dummy’s injury severity was greater than that of the head-on collision when the crash speed was 70 kph and lower. For high-velocity offset impact, the car’s rear tended to slither about the side of the rigid wall after the crash. A higher femur injury probability was observed due to the high axial force exerted by the deformation of the passenger compartment and intrusion.

Still, the oversteer effect lowered the head and neck injury probabilities. The chest injury at each impact velocity was not significantly different for the full-frontal and offset-frontal crashes because the compressive force from the seatbelt predominantly caused the injury.

4.3. Dummy Kinematics and Injury Severity in Car-to-Car Collision

The kinematics of the driver dummy in the L7e vehicle during the car-to-car full-frontal and 50% offset crash accident with the sedan model at an impact velocity of 50 kph is shown in Figure 18. The dummy tended to move forward after the initial impact due to the inertia of the dummy's head and limbs, where the body was restrained by a safety belt. A high head acceleration occurred when the flexion posture was initiated at 80 ms. At the same time, neck tension force and neck moments were maximized because the neck was pulled and rotated by the dummy's head inertia. A head-to-knee impact interaction occurred when the belted dummy's upper torso rotated over the shoulder belt, especially in the case of a high-velocity impact.

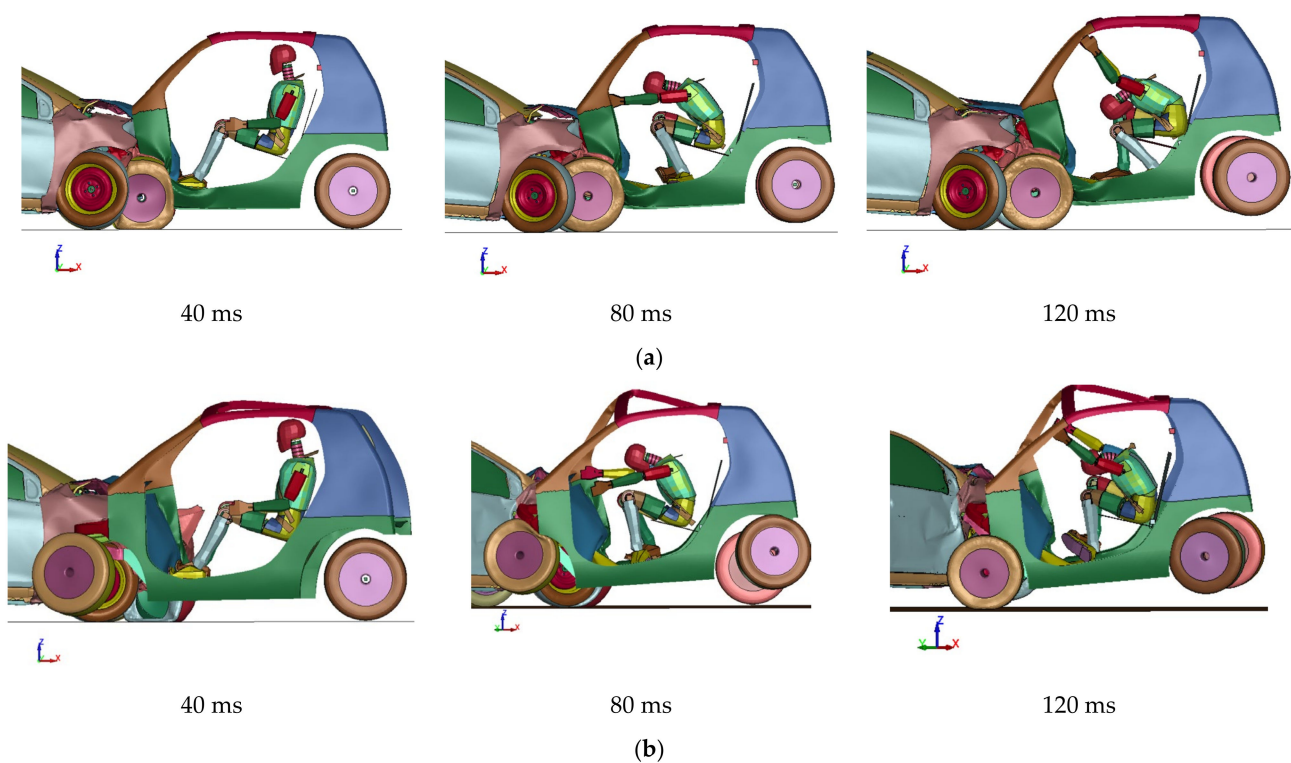


Figure 18. Typical kinematics of occupant dummy in L7e vehicle under full-frontal crash with a sedan: (a) full-frontal impact; (b) 50% offset impact.

The two-dimensional trajectories of the dummy's head and knee in the case of the full-frontal impact with the rigid wall are plotted in Figure 19. It can be seen that the proposed residual space was appropriate for preliminarily assessing the occupant injury severity. Additionally, the kinematics of the head trajectory also correlated with the results in Figure 16. The maximum head acceleration coincided with the high negative neck moment when the dummy's head moved forward, causing neck flexion until the head impacted the knee. The dummy injury probabilities were less than 20% for all the cases where the dummy's parts stayed inside the residual space, representing passenger safety. No structural components intruded into the assigned residual space when the impact velocities were 30 kph and 50 kph. However, the injury risk could not be quantitatively determined by the intrusion into the residual space in the case of the car-to-car collision. Injury results can be drastically different even when the intrusions are similar due to the complex behaviors of the energy absorption and structural characteristics during crashes with a low- and high-speed impact.

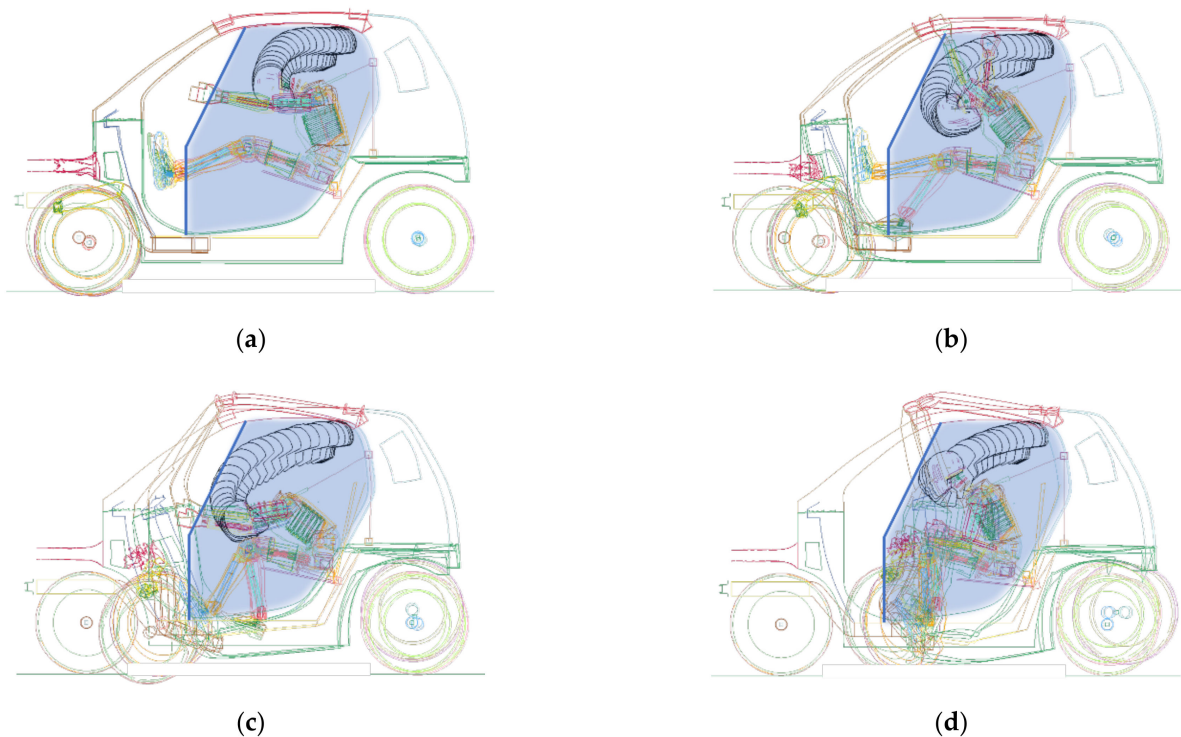


Figure 19. Dummy head and knee trajectories during the frontal crash: (a) 30 kph; (b) 50 kph; (c) 70 kph; (d) 90 kph.

A comparison of the dummy responses between crashing with the full-frontal rigid wall and car-to-car collisions with the sedan and SUV is shown in Figure 20. It can be seen that crashing the L7e vehicle with the rigid wall caused the lowest body forces and injury severity compared with the others due to the lowest impact energy from the lower mass of the quadricycle. Similar results were also observed in the case of the 50% offset crashes. Although standards and regulations generally require a vehicle's structural strength certification by an impact test to the rigid wall, the test might not be adequate to guarantee the safety of the L7e vehicle in actual car-to-car accidents. Thus, another crash test better replicating car-to-car crash tests should also be included in vehicle design and considerations of occupant safety.

When crashing with the sedan, the injury probability was significantly higher when the L7e vehicle's bumper height was high (Figure 21a), corresponding with the failure mode of the PEAS discussed in Section 3 and resulting in a high absorbed energy and a minimal deformation of L7e vehicle's frontal structure. At a low-speed impact, the full-frontal collision caused higher occupant injuries than the offset crash, where the head and neck were the most prevalent areas of injury. The offset-frontal crash at a high speed affected the femur injury due to the large deformation of the frontal structures' impact side, causing a striking increase in the femur forces. The chest deflections also tended to increase with the impact velocity, in which the probability of the AIS 2+ injury was up to 80% due to the seatbelt's restraint force. Thus, when the L7e car collided with the sedan, the low bumper height offered crashworthiness to the structure and the highest safety to the occupant dummy.

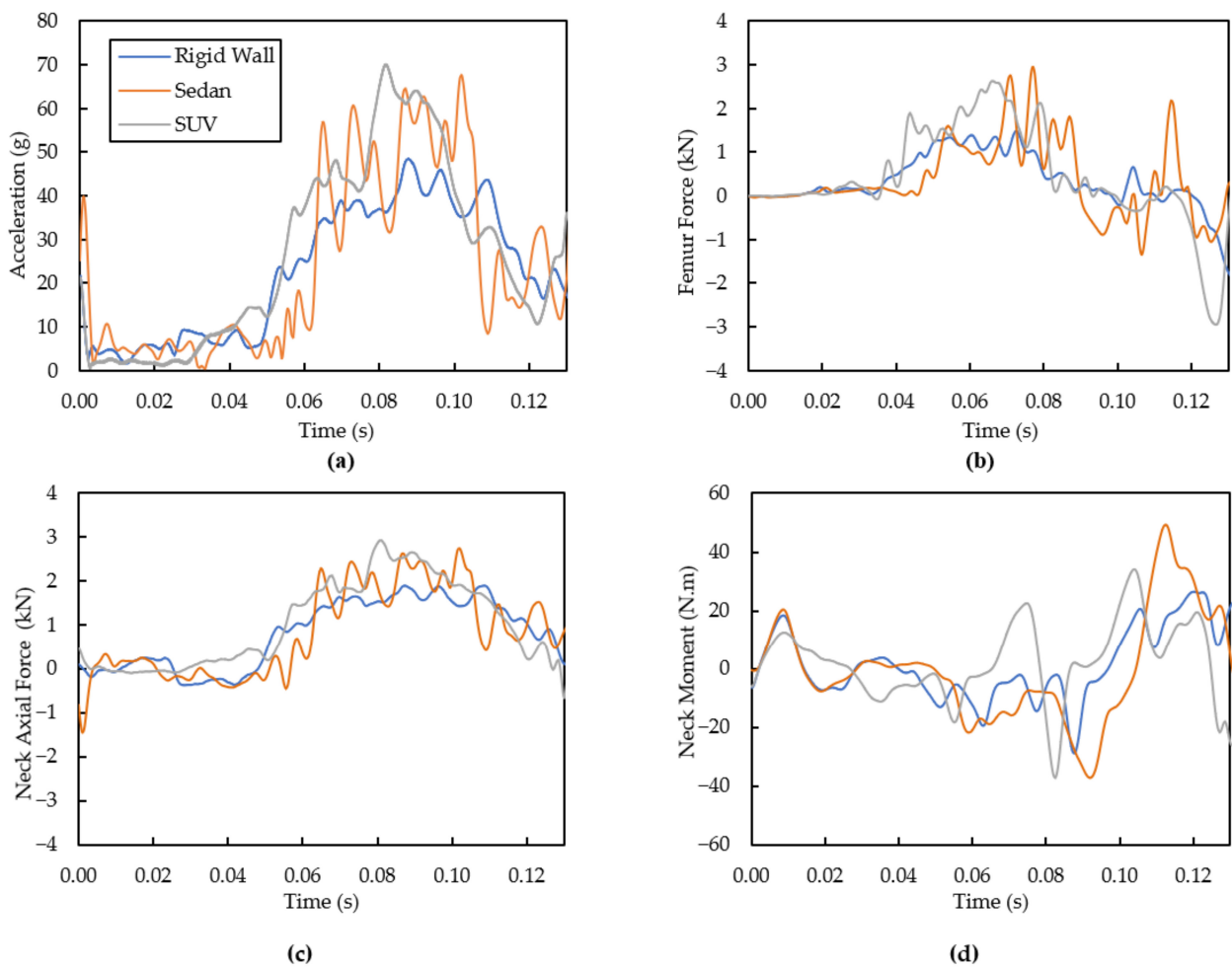


Figure 20. Dummy responses from full-frontal crashes with rigid wall and other opponent cars: (a) head acceleration; (b) femur forces; (c) neck axial forces; (d) neck axial moments.

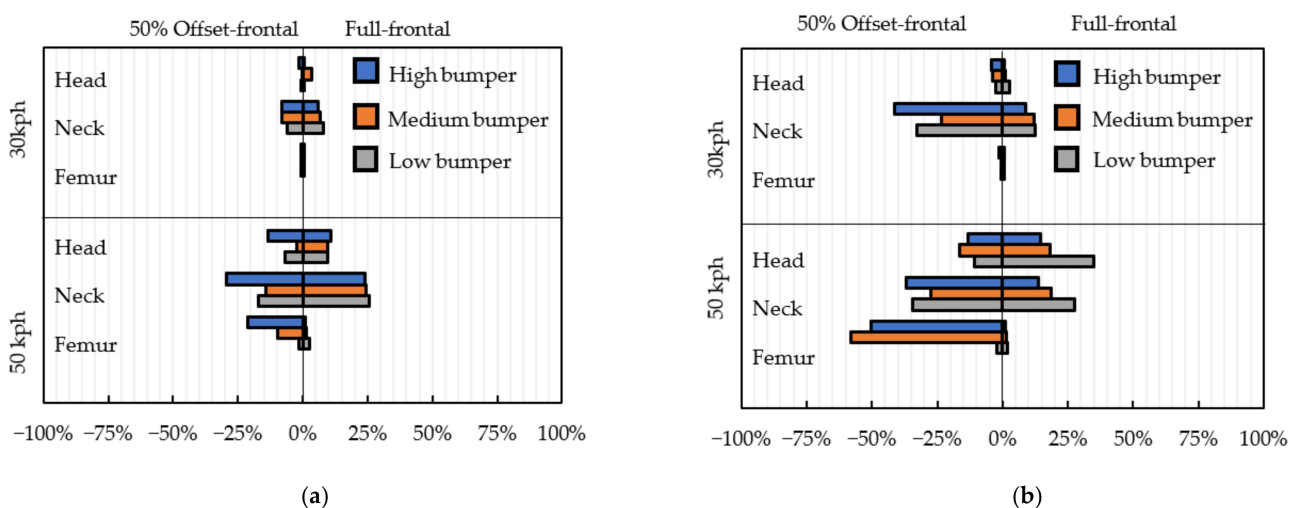


Figure 21. Injury severities from the car-to-car collision with: (a) the sedan; (b) the SUV.

Nevertheless, when the L7e vehicle crashed into the SUV, offset crashes caused more severe injury in the low- and high-speed crashes (Figure 21b). Although the discrepancy between different bumper heights was not as prominent as in the case of crashing with the sedan, the high bumper height was preferable in reducing the biomechanical forces of the

dummy. These results agreed well with the previous structural assessment, in which the quadricycle underrotated the SUV when the bumper height was low.

The different results of the car-to-car collisions with the sedan and SUV models for various bumper heights emphasize the importance of the compatible vertical alignment of the L7e vehicle's PEAS with the opponent vehicle to determine the occupant injury severity during an accident. A secondary energy-absorbing component could also be adapted to achieve vertical alignment with different vehicle sizes. In addition, the bumper's width should be increased to improve the quadricycle's protection in offset crashes. Proper dimensions and positions of the primary and secondary bumpers of the quadricycle to efficiently mitigate the occupant injury during various cases of the frontal crash should be further investigated.

5. Conclusions

This study investigates the crash behaviors of an electric heavy quadricycle under different crash scenarios with a rigid wall and in car-to-car crashes. Structural assessments and occupant injury assessments were employed to assess the protective performance of the L7e vehicle. The findings of this research can be concluded as follows:

- Under a frontal crash, the front rail should be able to fail in buckling mode to absorb high-impact energy and efficiently reduce the structural intrusion into the compartment zone.
- The crash compatibility of the quadricycle with other opponent vehicles for occupant safety is considerably affected by the vertical alignment of the primary energy-absorbing structure. Optimizing the appropriate vertical alignment to match the bumper within the part 581 zone and adding a secondary energy-absorbing structure to the L7e vehicle is recommended.
- The proposed residual space was well utilized to assess the structural performance and passenger safety in the full-frontal impact with the rigid wall scenario.
- The frontal impact of a quadricycle with the rigid wall might not be adequate to guarantee the occupant injuries from the actual car-to-car accidents since it showed the lowest injury severities compared with other car-to-car crashes.
- Safety assessments using only the energy absorption or intrusion of the frontal structures are inadequate to represent the passenger's injury severity because the results are significantly conflicted with the occupant injuries according to the AIS 2+.

Author Contributions: Conceptualization, P.J. (Pattaramon Jongpradist) and S.K.; methodology, P.J. (Pattaramon Jongpradist) and S.K.; software, T.H., N.T. and C.P.; validation, T.H. and N.T.; formal analysis, T.H., N.T. and C.P.; investigation, S.K.; resources, S.K.; data curation, S.K.; writing—original draft preparation, T.H.; writing—review and editing, S.K., P.J. (Pornkasem Jongpradist) and P.J. (Pattaramon Jongpradist); visualization, S.K.; supervision, P.J. (Pattaramon Jongpradist); project administration, T.H.; funding acquisition, S.K., P.J. (Pattaramon Jongpradist) and P.J. (Pornkasem Jongpradist). All authors have read and agreed to the published version of the manuscript.

Funding: This research and the APC were funded by the Research Strengthening Project, Faculty of Engineering, King Mongkut's University of Technology Thonburi.

Informed Consent Statement: Not applicable.

Data Availability Statement: Not applicable.

Conflicts of Interest: The authors declare no conflict of interest.

Appendix A

The finite element models of two types of vehicles, i.e., a sedan and an SUV, were studied and validated based on an impact analysis with a rigid wall. The models of the 2010 Toyota Yaris sedan and the 1997 Toyota Rav4 SUV used in the current study were developed by the National Crash Analysis Center. The final deformations of the sedan and SUV after crashing into the rigid wall while traveling less than 56 km/h were illustrated

in Figures A1 and A2, respectively. The deformations are in good agreement with experimental crash tests of the Toyota Yaris [28] and Toyota Rav4 [29].

Figures A3 and A4 show accelerations and impact force comparisons between the results obtained from the current simulation and experiments conducted by [30,31]. Decelerations at three target positions (left rear seat, right rear seat, and top engine) and the rigid wall force were measured to validate the crash simulation.

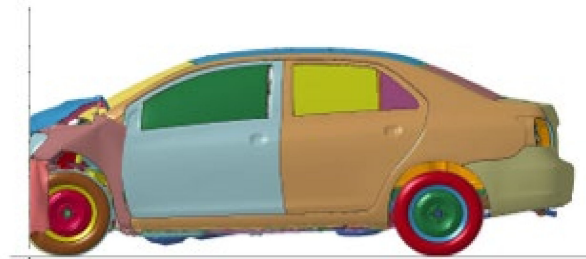


Figure A1. Simulation results of the frontal deformation of the sedan when impacting a rigid wall at 56 km/h speed.



Figure A2. Simulation results of the frontal deformation of the SUV when impacting a rigid wall at 56 km/h speed.

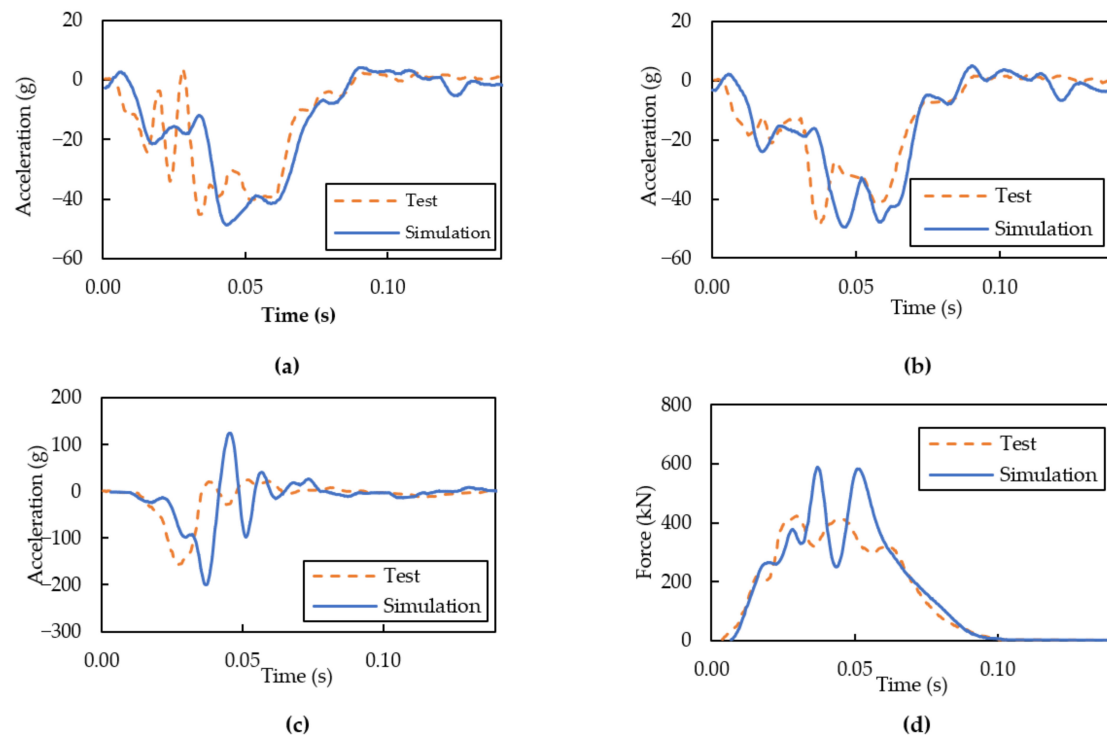


Figure A3. Deceleration results at target positions and rigid wall force of the Toyota Yaris model: (a) left rear seat; (b) right rear seat; (c) top engine; (d) rigid wall force.

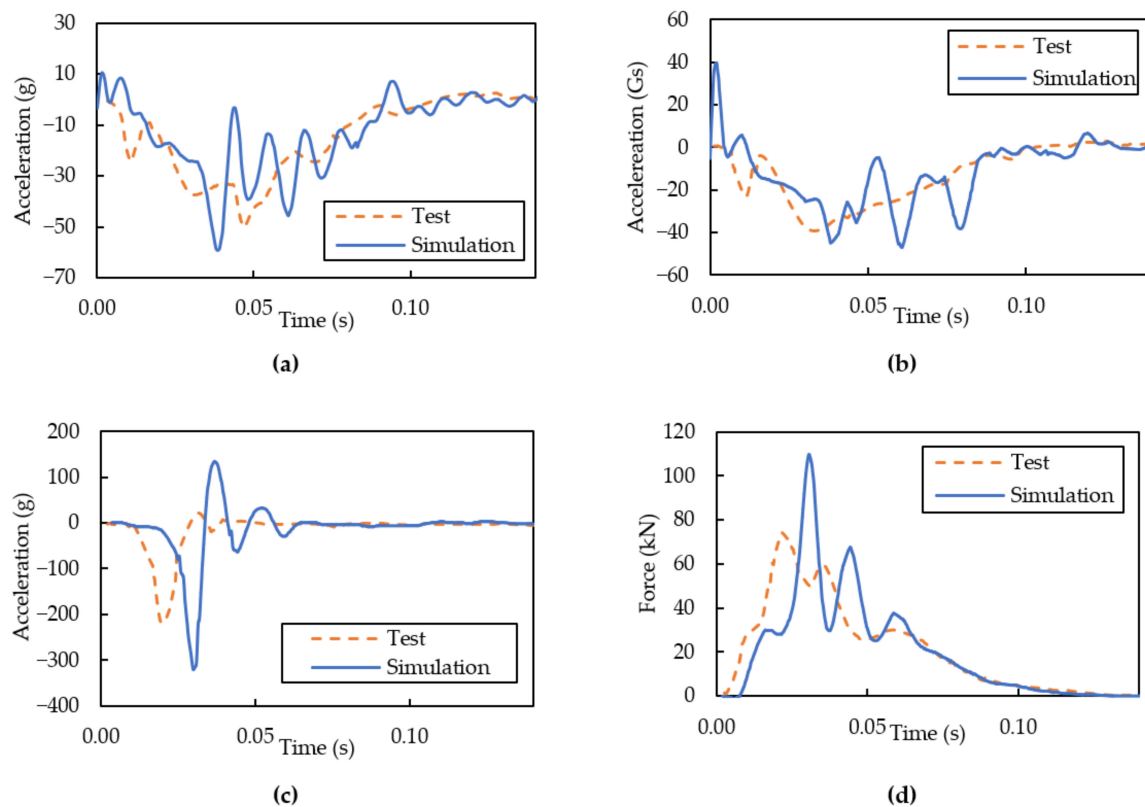


Figure A4. Deceleration results at target positions and rigid wall force of the Toyota Rav4 model: (a) left rear seat; (b) right rear seat; (c) top engine; (d) rigid wall force.

The Roadside Safety Verification and Validation Program (RSVVP) is an analytical tool utilized to statistically quantify the consistency between the test and simulation results [41]. The Sprague-Geers MPC metrics were used to guarantee the similarity of the deceleration curves in which a difference of less than 40% was acceptable for both magnitude and phase. In addition, ANOVA metrics were used to investigate the residual error, where the average deviation and standard deviation should not exceed 5% and 20%, respectively. The analytical results of the Toyota Yaris and Rav4 models at all the target positions are displayed in Tables A1 and A2. All the results passed the requirements of both the Sprague-Geers MPC and ANOVA conditions.

Table A1. Comparison of deceleration results and rigid wall force on RSVVP of the Toyota Yaris model.

Parameters		Left Rear Seat	Right Rear Seat	Top Engine	Rigid Wall Force
Sprague-Geers MPC	Magnitude (%)	−9.6	4.6	25.5	12.0
	Phase (%)	13.5	13.8	40.0	9.7
ANOVA	Average deviation (%)	−2.0	−1.6	−0.7	3.0
	Standard deviation (%)	17.1	18.7	33.2	16.9

Table A2. Comparison of deceleration results and rigid wall force on RSVVP of the Toyota Rav4 model.

Parameters		Left Rear Seat	Right Rear Seat	Top Engine	Rigid Wall Force
Sprague-Geers MPC	Magnitude (%)	−6.4	5.5	35.5	4.8
	Phase (%)	14.7	19.0	13.9	8.5
ANOVA	Average deviation (%)	3.5	2.6	0.7	9.8
	Standard deviation (%)	17.3	27.2	12.1	10.9

For the ATDs validation, the cushion of the passenger’s seat was neglected in the FE model, but the rigid seat was assigned to the simulation. The hybrid III 50th percentile male dummy was also validated based on the frontal sled test performed by [16]. The FE set-up is shown in Figure A5 with the assigned crash pulse of 30 km/h. The numerical results are shown in Figures A6 and A7. The maximum forces of the shoulder belt and lap belt from the simulation were different, around 7% and 20%, respectively. Therefore, the simulation of both the vehicle crashes and dummy occupants can represent the physical behaviors by comparing them with the test results, and they can be assured based on the acceptance criteria of the RSVVP.

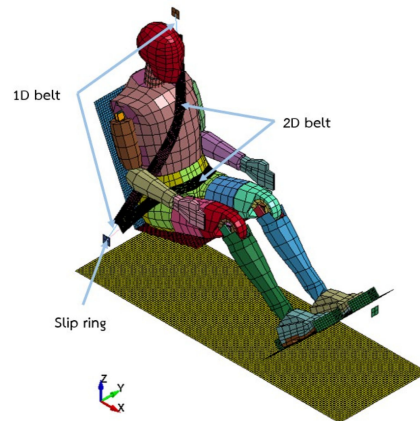


Figure A5. Completed FE model of frontal sled test for dummy validation.

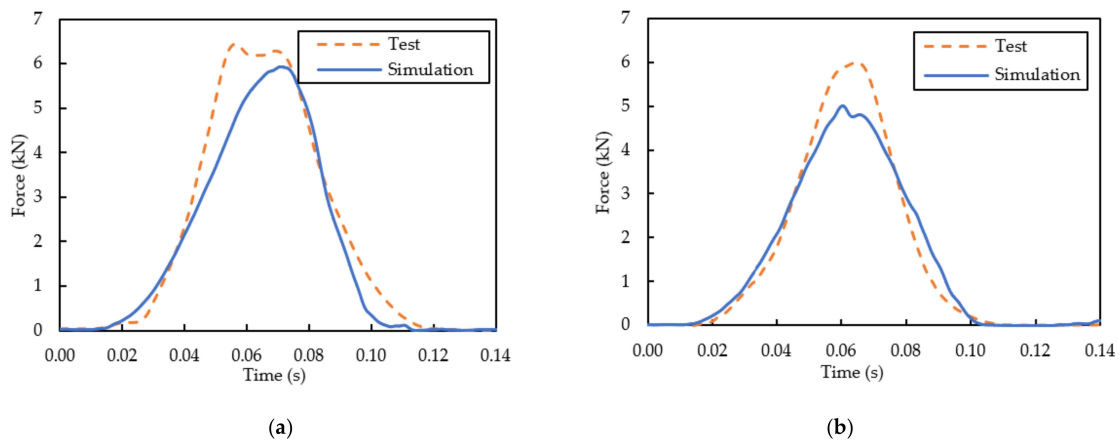


Figure A6. Comparison of seat belt forces of frontal sled test: (a) shoulder belt; (b) lap belt.

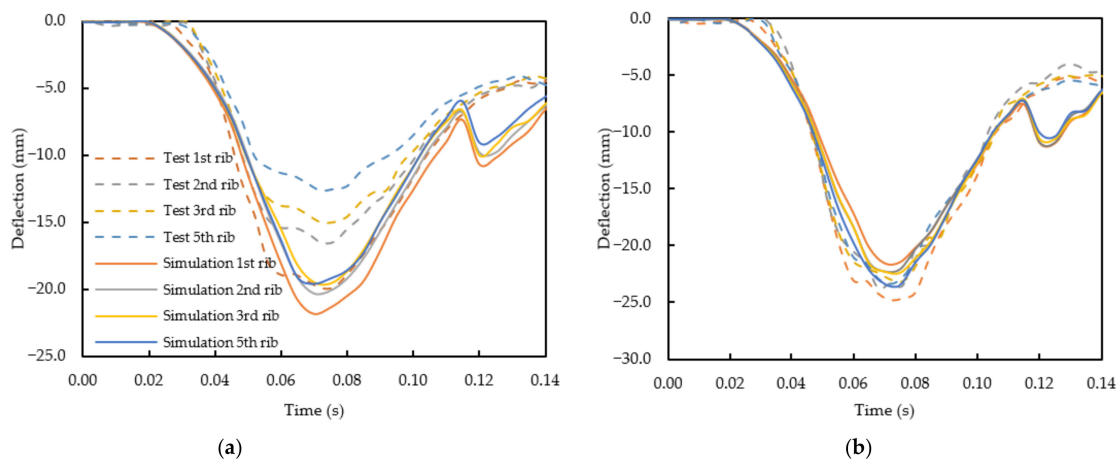


Figure A7. Comparison of rib deflections of frontal sled test: (a) left side; (b) right side.

Appendix B

The car-to-car collision simulation must be verified and validated by comparing the FE results via LS-DYNA with the calculations. A theoretical analysis, the so-called “Routh method,” was used to determine the impulses and directions of the angular velocity (ω) of each vehicle after the collision [36]. The impulses were measured in the normal and tangent directions of the collision plane (Figure A8). Meanwhile, the directions of the angular velocity in the vertical axis through the center of gravity (Figure A9) were considered.

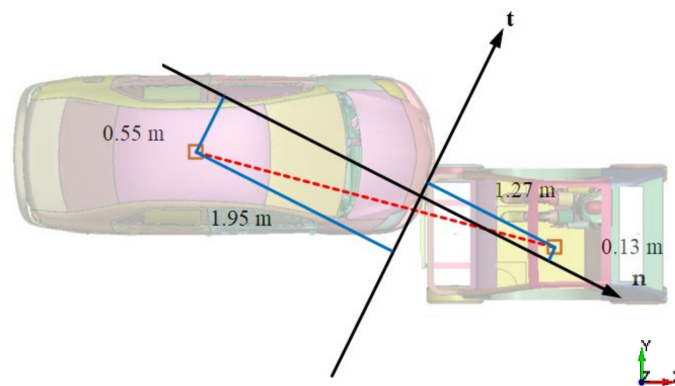


Figure A8. Distance from the center of the collision plane in the normal and tangent directions.

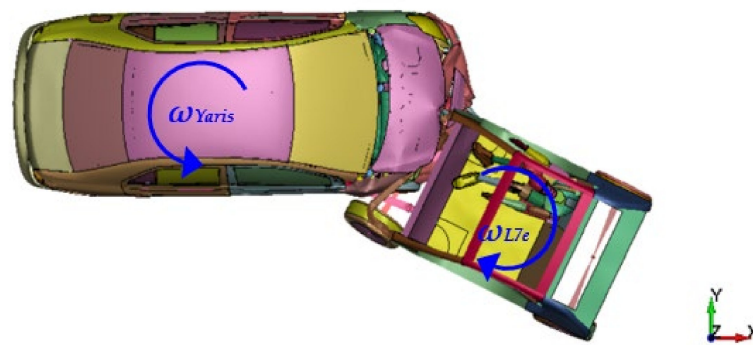


Figure A9. Directions of the angular velocity of each vehicle.

The impulses in the normal (S_n) and tangent (S_t) directions can be calculated using Equations (A1) and (A2), respectively, where f is the dynamic coefficient of friction and R is the restitution coefficient. The coefficients ϵ , ϑ , and i are required to evaluate the impulses by using Equations (A3)–(A5). The variables v , ω , m , I_{zz} , and t are the translational velocity, the angular velocity, the vehicle’s mass, the moment of inertia at the vertical axis through the vehicle’s center of gravity, and the distance between the center of the collision and the center of gravity of each vehicle in the tangent axis, respectively.

$$S_n = (1 + R) \bullet \epsilon \quad (\text{A1})$$

$$S_t = f \bullet S_n \quad (\text{A2})$$

$$\epsilon = \frac{[(v_{Yaris,n} + \omega_{Yaris} t_{Yaris}) - (v_{L7e,n} + \omega_{L7e} t_{L7e})] \cdot m_{Yaris} \cdot m_{L7e}}{(1 + \vartheta_{L7e}^2) \cdot m_{Yaris} + (1 + \vartheta_{Yaris}^2) \cdot m_{L7e}} \quad (\text{A3})$$

$$\vartheta = \frac{t}{i} \quad (\text{A4})$$

$$i = \sqrt{\frac{I_{zz}}{m}} \quad (\text{A5})$$

The simulation and analytical results are compared in Table A3 for the 50% offset car-to-car crash between the L7e vehicle and Toyota Yaris at 30 kph, where m_{Yaris} and m_{L7e}

are 1263 kg and 790 kg, respectively. The parameters f and R are equal to 0.2 and 0.98, respectively. The simulation results are in fair agreement with those of the analytical results from the Routh method, although the impulses and angular velocities from the theoretical analysis are slightly smaller.

Table A3. Results comparison between simulation via LS-DYNA and theoretical calculation using the Routh method.

Post-Crash Result	Simulation	Theoretical
Normal impulse (N.s)	8963	8155
Tangent impulse (N.s)	1539	1631
Resultant impulse (N.s)	9094	8316
ω_{Yaris} (1/s)	0.71	1.29
ω_{L7e} (1/s)	−4.40	−2.06

References

- Choma, E.F.; Evans, J.S.; Hammitt, J.K.; Gómez-Ibáñez, J.A.; Spengler, J.D. Assessing the health impacts of electric vehicles through air pollution in the United States. *Environ. Interact.* **2020**, *144*, 106015. [CrossRef] [PubMed]
- Mu, R.; Yamamoto, T. An analysis on mixed traffic flow of conventional passenger cars and microcars using a cellular automata model. *Procedia-Soc. Behav. Sci.* **2012**, *43*, 457–465. [CrossRef]
- Wüstenhagen, S.; Beckert, P.; Lange, O.; Franze, A. Light Electric Vehicles for Muscle–Battery Electric Mobility in Circular Economy: A Comprehensive Study. *Sustainability* **2021**, *13*, 13793. [CrossRef]
- Redelbach, M.; Özdemir, E.D.; Friedrich, H.E. Optimizing battery sizes of plug-in hybrid and extended range electric vehicles for different user types. *Energy Policy* **2014**, *73*, 158–168. [CrossRef]
- The European New Car Assessment Programme. 2016 Quadricycles' Tests. Available online: <https://www.euroncap.com/en/vehicle-safety/safety-campaigns/2016-quadricycles-tests> (accessed on 13 December 2021).
- Kongwat, S.; Jaroenjittakam, S.; Chaianan, S.; Atchariyauthen, I.; Jongpradist, P. Design for crash safety of electric heavy quadricycle structure. *IOP Conf. Ser. Mater. Sci. Eng.* **2021**, *1137*, 012012. [CrossRef]
- Wolsfeld, R.; Klein, F.; Seidel, K.; Zehnpfennig, L. Concept of an L7e microcar with high passive safety. *Lightweight Des. Worldw.* **2018**, *11*, 30–35. [CrossRef]
- Setiawan, R.; Salim, M.R. Crashworthiness Design for an Electric City Car against Side Pole Impact. *J. Eng. Technol. Sci.* **2017**, *49*, 587–603. [CrossRef]
- Sadeghipour, E. A New Approach to Assess and Optimize the Frontal Crash Compatibility of Vehicle Structures. Ph.D. Thesis, Technische Universität München, Munich, Germany, 2017.
- Sandner, V.; Ratzek, A. MPDB-Mobile offset progressive deformable barrier. In Proceedings of the 24th International Technical Conference on the Enhanced Safety of Vehicles (ESV), Gothenburg, Sweden, 8–11 June 2015.
- Dios, E.; Lázaro, I.; Delannoy, P.; Thomson, R.; Versmissen, T.; Nunen, E. Development of a structural interaction assessment criteria using progressive deformable barrier data. In Proceedings of the 23rd International Technical Conference on the Enhanced Safety of Vehicles (ESV), Seoul, Korea, 27–30 May 2013.
- Johannsen, H.; Adolph, T.; Thomson, R.; Edwards, M.; Lázaro, I.; Versmissen, T. Fimcar—Frontal impact and compatibility assessment research: Strategy and first results for future frontal Impact Assessment. In Proceedings of the 22nd ESV Conference Proceedings, Washington, DC, USA, 13–16 June 2011.
- Zeng, Q.; Wen, H.; Huang, H. The interactive effect on injury severity of driver-vehicle units in two-vehicle crashes. *J. Saf. Res.* **2016**, *59*, 105–111. [CrossRef]
- Huang, H.; Siddiqui, C.; Abdel-Aty, M. Indexing crashworthiness and crash aggressivity by vehicle type. *Accid. Anal. Prev.* **2011**, *43*, 1364–1370. [CrossRef]
- Thompson, A.; Edwards, M.; Wisch, M.; Adolph, T.; Krusper, A.; Thomson, R.; Johannsen, H. *Report Detailing the Analysis of National Accident Databases*; FP7 European Commission FIMCAR Project; GA (234216); Springer: Berlin, Germany, 2011.
- Eggers, A.; Adolph, T. Evaluation of the Thoracic Deflection Measurement System 'RibEye' in the Hybrid III 50th in Frontal Sled Tests. In Proceedings of the 23rd International Technical Conference on the Enhanced Safety of Vehicles (ESV), Seoul, Korea, 27–30 May 2013.
- Lemmen, P.; Hynd, D.; Carroll, J.; Davidsson, J.; Been, B.; Song, E.; Steeger, B. Thoracic Injury Assessment for Improved Vehicle Safety. *Procedia-Soc. Behav. Sci.* **2012**, *48*, 1649–1661. [CrossRef]
- Hallman, J.J.; Yoganandan, N.; Pintar, F.A.; Maiman, D.J. Injury Differences Between Small and Large Overlap Frontal Crashes. *Ann. Adv. Automot. Med.* **2011**, *55*, 147–157. [PubMed]
- Kolke, R.; Sandner, V.; Ambos, R.; Unger, T. Frontal and side impact compatibility. *ATZ Worldw.* **2010**, *112*, 18–24. [CrossRef]
- Sadeghipour, E.; Duddeck, F.; Lienkamp, M. Crash Compatibility of Microcars: A Study on Current Test Approaches. In Proceedings of the Crash. Tech. 2014, Munich, Germany, 8–9 April 2014. [CrossRef]

21. The European New Car Assessment Programme. Mobile Progressive Deformable Barrier. 2020. Available online: <https://www.euroncap.com/en/vehicle-safety/the-ratings-explained/adult-occupant-protection/frontal-impact/mobile-progressive-deformable-barrier> (accessed on 13 December 2021).
22. Davies, H.C.; Bastien, C. An approach for the crash safety assessment of smaller and lightweight vehicles. *Transp. Policy* **2021**, *105*, 12–21. [[CrossRef](#)]
23. Dux, L.E.E.; Wolkenstein, M.; Luttenberger, P. A Mobile Deformable Barrier Test for the Front Crash Assessment of Future Urban Microcars. In Proceedings of the 24th International Technical Conference on the Enhanced Safety of Vehicles (ESV), Gothenburg, Sweden, 8–11 June 2015.
24. Zhendong, S.; Haitao, Z.; Weiqiang, P. Assessment of Car to Car crash compatibility based on MPDB. In Proceedings of the 12th International Conference on Measuring Technology and Mechatronics Automation (ICMTMA), Phuket, Thailand, 28–29 February 2022. [[CrossRef](#)]
25. Baker, B.C.; Nolan, J.M.; O’Neill, B.; Genetos, A.P. Crash compatibility between cars and light trucks: Benefits of lowering front-end energy-absorbing structure in SUVs and pickups. *Accid. Anal. Prev.* **2008**, *40*, 116–125. [[CrossRef](#)] [[PubMed](#)]
26. O’Brien, S. Priorities for the assessment of frontal impact compatibility. In Proceedings of the 22nd International Technical Conference on the Enhanced Safety of Vehicles, Washington, DC, USA, 13–16 June 2011.
27. Yonezawa, H. Investigation for New Side Impact Test Procedures in Japan. In Proceedings of the 21st International Technical Conference on the Enhanced Safety of Vehicles, Stuttgart, Germany, 15–18 June 2009.
28. Fischer, B. *Final Report of New Car Assessment Program Testing of a 2007 Toyota Yaris*; MGA Research Corporation: Burlington, WI, USA, 2006.
29. Sankey, J.W. *Final Report of New Car Assessment Program Testing of a 1997 Toyota RAV4*; Transportation Research Center Inc.: East Liberty, OH, USA, 1997.
30. Marzougui, D.; Samaha, R.R.; Nix, L.; Kan, C.D.S. *Extended Validation of the Finite Element Model for the 2010 Toyota Yaris Passenger Sedan (MASH 1100 kg Vehicle)*; Working Paper NCAC 2012-W-005; National Crash Analysis Center (NCAC): Ashburn, VA, USA, 2012.
31. National Crash Analysis Center (NCAC). *Finite Element Model of Toyota Rav 4 (The Model Year 1997)*; National Crash Analysis Center (NCAC): Ashburn, VA, USA, 2008.
32. Li, S.; Sui, J.; Ding, F.; Wu, S.; Chen, W.; Wang, C. Optimization of Milling Aluminum Alloy 6061-T6 using Modified Johnson-Cook Model. *Simul. Model. Pract. Theory* **2021**, *111*, 102330. [[CrossRef](#)]
33. Ansys Company. Livermore Software Technology. Hybrid III 50th Percentile Male. Available online: https://www.lstc.com/products/models/dummies/H3_50th (accessed on 16 November 2020).
34. Yeh, I. LS-DYNA Seatbelt Modeling Guideline. 2007. Available online: https://ftp.lstc.com/anonymous/outgoing/support/FAQ_docs/SeatBeltGuideline1.pdf (accessed on 9 June 2022).
35. Chou, C.C.; Nyquist, G.W. Analytical Studies of the Head Injury Criterion (HIC). *SAE Trans.* **1974**, *83*, 398–410.
36. Zalewski, J.; Kisilowski, J. Analysis of Chosen Aspects of a Two-Car Crash Simulation. In Proceedings of the International Conference on Transport Systems Telematics, Ustron, Poland, 10–13 October 2012; pp. 34–44.
37. Christensen, J.; Bastien, C. *Nonlinear Optimization of Vehicle Safety Structures: Modeling of Structures Subjected to Large Deformations*; Butterworth-Heinemann: Oxford, UK, 2015.
38. Association for the Advancement of Automotive Medicine. *The abbreviated Injury Scale 2015 Revision*; Association for the Advancement of Automotive Medicine: Des Plaines, IL, USA, 2016.
39. Lesko, M.M.; Woodford, M.; White, L.; O’Brien, S.J.; Childs, C.; Lecky, F.E. Using Abbreviated Injury Scale (AIS) codes to classify Computed Tomography (CT) features in the Marshall System. *BMC Med. Res. Methodol.* **2010**, *10*, 72. [[CrossRef](#)] [[PubMed](#)]
40. Eppinger, R.; Sun, E.; Bandak, F.; Haffner, M.; Khawepong, N.; Maltese, M.; Kuppa, S.; Nguyen, T.; Takhounts, E.; Tannous, R.; et al. *Development of Improved Injury Criteria for the Assessment of Advanced Automotive Restraint Systems—II*; NHTSA: Washington, DC, USA, 1999.
41. Ray, M.H.; Mongiardini, M.; Atahan, A.O.; Plaxico, C.A.; Anghileri, M. *Recommended Procedures for Verification and Validation of Computer Simulations Used for Roadside Safety Applications*; National Cooperative Highway Research Program (NCHRP): Washington, DC, USA, 2008.